IET Electric Power Applications

Research Article

IET Journals
The Institution of Engineering and Technology

Hybrid predictive control strategy for a low-cost converter-fed IM drive

ISSN 1751-8660
Received on 16th September 2017
Revised 13th January 2018
Accepted on 25th January 2018
E-First on 27th February 2018
doi: 10.1049/iet-epa.2017.0587
www.ietdl.org

Shuqi Shi[1,2], Yao Sun[1] ✉, Mei Su[1], Ruyu Che[1]

[1]*School of Information Science and Engineering, Central South University, Changsha, People's Republic of China*
[2]*Hunan Provincial Key Laboratory of Grids Operation and Control on Multi-Power Sources Area, Shaoyang University, Shao yang, People's Republic of China*
✉ *E-mail: yaosuncsu@gmail.edu.com*

Abstract: The converter consisting of a single-phase half-bridge rectifier and four-switch three-phase inverter is a low-cost power converter with complicated operating constraints. It is difficult to control by the conventional strategies. This study proposes a hybrid predictive control strategy with dual loops for this converter. In the outer loop, a proportional–integral controller is designed to regulate the dc-link voltage, capacitor voltage balancing, and the speed and flux of induction motors (IM). Also, in the inner loop, the finite set model predictive control is employed to control the ac input current and stator currents of the IM. The major advantages of the control strategy include: (i) easy to deal with complicated constraints and manage multiple control targets; (ii) without the need of modulators; (iii) good dynamic response. The simulation and experimental results indicate that the proposed method can guarantee the stable operation and good performance.

1 Introduction

The single-phase input three-phase output converter-fed induction motor (IM) drive has attracted much attention due to its advantages of low cost, simple structure, high power density, and efficiency [1, 2]. Thus, it has been found widespread household application in various forms. Typical applications include the fans, air-compressors, pumps etc.

In order to decrease the costs and improve the reliability of power conversion systems, some simplified topologies of single-phase input three-phase output converters are proposed [3]. In Fig. 1*a*, the third bridge arm is multiplexed between converters A and B. Fig. 1*b* shows a more simplified converter where the capacitor bridge arm is multiplexed between converters A and B. Compared the converter in Fig. 1*a*, the converter in Fig. 1*b* requires fewer switching devices. However, the coupling and constraints are enhanced, which increases control difficulty of the converter.

Lots of control methods for the single-phase input three-phase output converter have been proposed. In most cases, the rectifier part and the inverter part are controlled separately, while the way to treat them together has not been reported. Usually, the control architecture of the converter could be divided into modulation and control. In the rectifier part, the current control is very essential to obtain good performance. The hysteresis control and carrier-based modulation methods have been proposed [4–7]. The hysteresis current control is simple, but the frequency is unfixed and current total harmonic distortion (THD) is relatively high. The equivalence of space vector modulation (SVM) and carrier-based pulse width modulation (PWM) in three-phase rectifier is studied in detail [3]. On the basis of the equivalence, a carrier-based modulation method is proposed [4]. To improve efficiency, some PWM methods are presented. In order to improve the output characteristics of the four-switch three-phase inverter, the corresponding PWM modulation schemes are proposed in [5–9]. The calculation expression of the power tube's switching time is proposed in [10, 11], but only linear processing. Consider the dead zone effect, the switching time compensation of the power switch tube is proposed in the literature [12]. A specific harmonic injection method is used to improve the voltage utilisation to a certain extent in [13], but the calculation is complex and lacks a clear analytic expression. To mitigate the effects of the capacitor voltage fluctuation, several papers were published. An adaptive SVM approach was proposed to compensate the dc-link voltage ripple in a four-switch three-phase inverter [14]. From the perspective of source impedance and

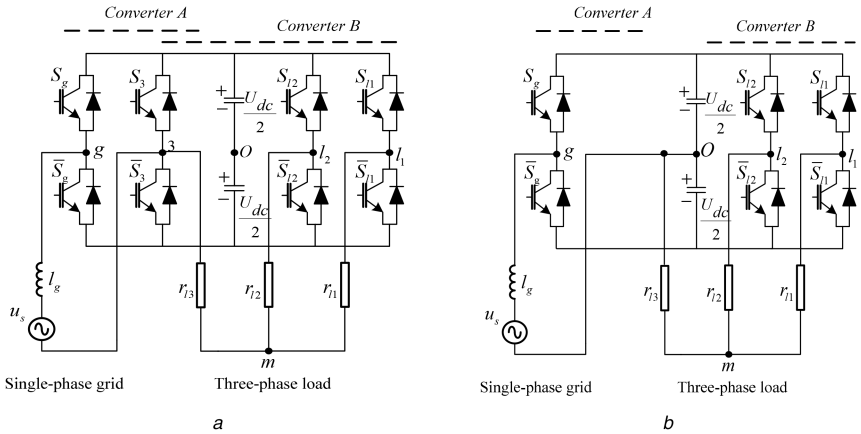

Fig. 1 *Simplified topological circuit*
(a) Single-phase input three-phase output full-bridge simplified topology, ***(b)*** Single-phase input three-phase output half-bridge simplified topology

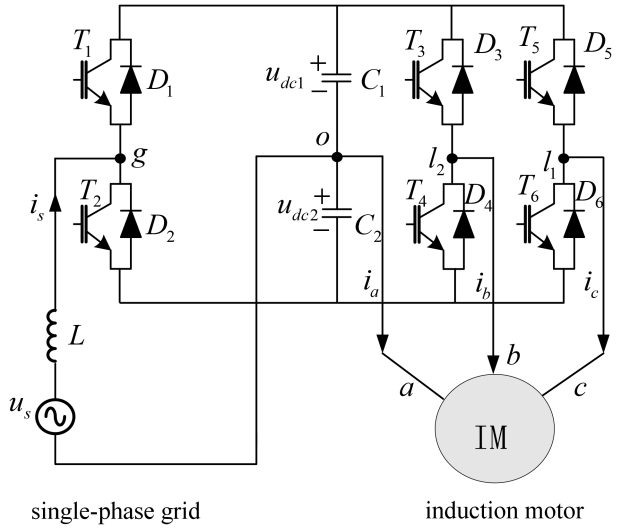

Fig. 2 *Topology with reduced switches converter*

the voltage variation caused by the current flowing through the capacitor, a current distortion compensation scheme is proposed [15]. In [16], a compensation method by adjusting switching times considering the capacitor voltage fluctuation is presented. The works mentioned earlier were dedicated to obtain the balanced three-phase currents of the inverter, but the inherent constraints were not considered.

As well known, the traditional model predictive control (MPC) has the advantage of handling constraints [17]. However, the general MPC is not much suitable for power electronic circuits which demands high performance of real time [18]. Recently, a finite set MPC (FS-MPC) scheme has been proposed for power converters [18–20]. The FS-MPC algorithm, which is easy to understand and flexible to control, can fully consider the constraint conditions of system and easily deal with them. In addition, it also can achieve various objectives by changing the form of the cost function, weight factor, and the number of variables. With multi-variable control capability, the rectifier and inverter part can be controlled together. The FS-MPC control treats the power converter as a discrete and non-linear actuator. In FS-MPC system, through a single controller to realise the control actions, which can select the status online from all possible states [21, 22].

In this study, a hybrid predictive control strategy which combines the FS-MPC and proportional–integral (PI) control is applied to control single-phase half-bridge rectifier and four-switch three-phase inverter. It enables the system to achieve the stable output, and can meet the high flexibility. The remainder of this paper is organised as follows: Section 2 presents the system model of the single-phase half-bridge rectifier and four-switch three-phase inverter. Section 3 presents the corresponding discrete model. The proposed control scheme is described in Section 4. In Section 5, the simulation and experimental results are shown, and finally, the conclusion is presented in Section 6.

2 System modelling

The studied single-phase input three-phase output converter is shown in Fig. 2, which is made up of six insulated gate bipolar transistors (IGBTs). IGBT T_1, T_2 and capacitor C_1, C_2 together constitute a single-phase half-bridge rectifier circuit, the remaining four IGBTs and the capacitor C_1, C_2 together form a low-cost four-switch three-phase inverter circuit. The rectifier provides the dc-link voltage for the inverter and the inverter is followed by a three-phase induction motor.

To facilitate modelling, denote S_i ($i = 1, 2, 3, 4, 5, 6$) as the switching state of the switch T_i ($i = 1, 2, 3, 4, 5, 6$) of the converter. Then, the dynamic equations of the input current, the two dc-link capacitor voltages, and the stator current can be obtained as follows:

$$L\frac{\mathrm{d}i_\mathrm{s}}{\mathrm{d}t} = u_\mathrm{s} - S_1u_\mathrm{dc1} + (1 - S_1)u_\mathrm{dc2} \tag{1}$$

$$C\frac{\mathrm{d}u_\mathrm{dc1}}{\mathrm{d}t} = S_1i_\mathrm{s} - S_3i_b - S_5i_c \tag{2}$$

$$C\frac{\mathrm{d}u_\mathrm{dc2}}{\mathrm{d}t} = C\frac{\mathrm{d}u_\mathrm{dc1}}{\mathrm{d}t} - i_a - i_\mathrm{s} \tag{3}$$

$$L_\delta\frac{\mathrm{d}i_a}{\mathrm{d}t} = u_{aN} - e_a - i_ar_\mathrm{s} \tag{4}$$

$$L_\delta\frac{\mathrm{d}i_b}{\mathrm{d}t} = u_{bN} - e_b - i_br_\mathrm{s} \tag{5}$$

$$L_\delta\frac{\mathrm{d}i_c}{\mathrm{d}t} = u_{cN} - e_c - i_cr_\mathrm{s} \tag{6}$$

where L is the grid-side inductance, and i_s and u_s are the ac source current and voltage, respectively. $C_1 = C_2 = C$ is the capacitor of the dc-link, u_dc1, u_dc2 are the upper and the lower dc-link voltages. u_{iN}, i_i, and e_i ($i = a, b, c$) are the stator phase voltage, phase current, back electromotive force of the IM, respectively. L_δ and r_s are the leakage inductance and stator resistance of the motor, respectively.

The stator phase voltage u_{aN}, u_{bN}, and u_{cN} of the induction motor can be expressed as

$$\begin{cases} u_{aN} = \dfrac{2}{3}u_\mathrm{dc2} - \dfrac{1}{3}S_3u_\mathrm{dc} - \dfrac{1}{3}S_5u_\mathrm{dc} \\ u_{bN} = \dfrac{2}{3}S_3u_\mathrm{dc} - \dfrac{1}{3}S_5u_\mathrm{dc} - \dfrac{1}{3}u_\mathrm{dc2} \\ u_{cN} = \dfrac{2}{3}S_5u_\mathrm{dc} - \dfrac{1}{3}S_3u_\mathrm{dc} - \dfrac{1}{3}u_\mathrm{dc2} \end{cases} \tag{7}$$

where u_dc is the total dc-link voltage.

For convenience, the equations formulated in *abc* coordinate should be transformed to $\alpha\beta$ coordinate. As equations in (4–6) are general expressions, the back electromotive force information should be formulated concretely. Thus, the dynamic equations for stator currents of the induction motor are rewritten as [23, 24]

$$\begin{cases} \dfrac{\mathrm{d}i_\alpha}{\mathrm{d}t} = -\gamma i_\alpha + \alpha\beta\psi_{r\alpha} + \beta p\omega\psi_{r\beta} + \dfrac{1}{\sigma}u_\alpha \\ \dfrac{\mathrm{d}i_\beta}{\mathrm{d}t} = -\gamma i_\beta + \alpha\beta\psi_{r\beta} - \beta p\omega\psi_{r\alpha} + \dfrac{1}{\sigma}u_\beta \end{cases} \tag{8}$$

where i_α and i_β are the stator α, β-axis currents; u_α and u_β represent the stator α, β -axis voltages; $\psi_{r\alpha}$ and $\psi_{r\beta}$ are the rotor α, β-axis flux; ω and p the rotor angular speed and the number of pole pairs, respectively. Constants related to electrical and mechanical parameters of IM are defined as: $\sigma = L_\mathrm{s}(1 - (L_\mathrm{m}^2)/(L_\mathrm{s}L_\mathrm{r}))$, $\gamma = (r_\mathrm{s}/\sigma) + \alpha L_\mathrm{m}\beta$, $\alpha = (r_\mathrm{r})/(L_\mathrm{r})$, $\beta = (L_\mathrm{m})/(\sigma L_\mathrm{r})$, r_s, r_r, L_s, L_r are stator/rotor resistance and inductance, respectively. L_m is the mutual inductance.

In (8), the rotor flux expressions are given as follows:

$$\begin{cases} \psi_{r\alpha} = \dfrac{1}{T_\mathrm{r}s + 1}\left(L_\mathrm{m}i_\alpha - \omega T_\mathrm{r}\psi_{r\beta}\right) \\ \psi_{r\beta} = \dfrac{1}{T_\mathrm{r}s + 1}\left(L_\mathrm{m}i_\beta + \omega T_\mathrm{r}\psi_{r\alpha}\right) \end{cases} \tag{9}$$

$$\psi_\mathrm{r} = \sqrt{\psi_{r\alpha}^2 + \psi_{r\beta}^2} \tag{10}$$

$$\theta = \arctan(\psi_{r\beta}/\psi_{r\alpha}) \tag{11}$$

where T_r is the rotor electromagnetic time constant, and ψ_r and θ are the amplitude and angle of rotor flux.

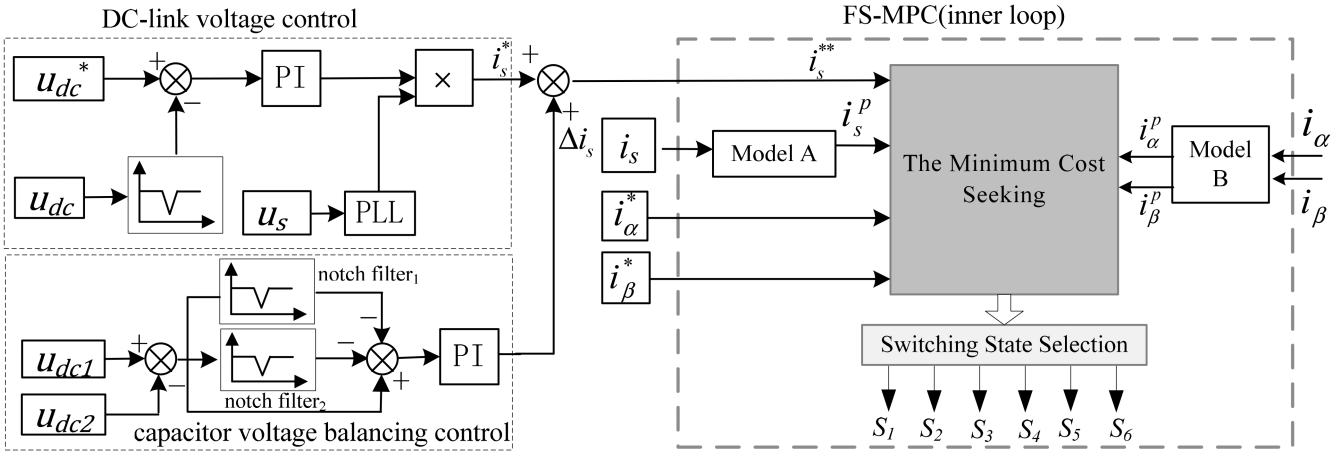

Fig. 3 *Control diagram of the proposed control strategy*

3 Discrete model

Assume that the sampling period t_s is relatively small. The forward Euler method is used to discretise the system. Then, the resulted discrete-time equations of (1), (2), (3), and (8) are described as

$$L\frac{i_s(k+1)-i_s(k)}{t_s}=u_s(k)-S_1u_{dc1}(k)+(1-S_1)u_{dc2}(k) \tag{12}$$

$$C\frac{u_{dc1}(k+1)-u_{dc1}(k)}{t_s}=S_1i_s(k)-S_3i_b(k)-S_5i_c(k) \tag{13}$$

$$C\frac{u_{dc2}(k+1)-u_{dc2}(k)}{t_s}=C\frac{u_{dc1}(k+1)-u_{dc1}(k)}{t_s}-i_s(k)-i_a(k) \tag{14}$$

$$\begin{cases}\dfrac{i_\alpha(k+1)-i_\alpha(k)}{t_s}=-\gamma i_\alpha(k)+\alpha\beta\psi_{r\alpha}(k)+\beta p\omega\psi_{r\beta}(k)+\dfrac{1}{\sigma}u_\alpha(k)\\ \dfrac{i_\beta(k+1)-i_\beta(k)}{t_s}=-\gamma i_\beta(k)+\alpha\beta\psi_{r\beta}(k)-\beta p\omega\psi_{r\alpha}(k)+\dfrac{1}{\sigma}u_\beta(k)\end{cases} \tag{15}$$

Then, the predicted values i_s^p, u_{dc1}^p, u_{dc2}^p, i_α^p, and i_β^p at instant $k+1$ are obtained, respectively

$$i_s^p=\frac{t_s}{L}[u_s(k)-S_1u_{dc1}(k)+(1-S_1)u_{dc2}(k)]+i_s(k) \tag{16}$$

$$u_{dc1}^p=\frac{t_s}{C}[S_1i_s(k)-S_3i_b(k)-S_5i_c(k)]+u_{dc1}(k) \tag{17}$$

$$u_{dc2}^p=\frac{t_s}{C}[(S_1-1)i_s(k)-S_3i_b(k)-S_5i_c(k)-i_a(k)]+u_{dc2}(k) \tag{18}$$

$$\begin{cases}i_\alpha^p=i_\alpha(k)+t_s\left[-\gamma i_\alpha(k)+\alpha\beta\psi_{r\alpha}(k)+\beta p\omega\psi_{r\beta}(k)+\dfrac{1}{\sigma}u_\alpha(k)\right]\\ i_\beta^p=i_\beta(k)+t_s\left[-\gamma i_\beta(k)+\alpha\beta\psi_{r\beta}(k)-\beta p\omega\psi_{r\alpha}(k)+\dfrac{1}{\sigma}u_\beta(k)\right]\end{cases} \tag{19}$$

4 Proposed control scheme

The targets of the whole control system are: (i) to achieve the unit power factor operation for the rectifier; (ii) to maintain the capacitor voltage balance; (iii) to regulate the speed of the IM. Fig. 3 shows the proposed control block diagram, which involves an outer loop control and an inner loop control.

4.1 Outer loop control

The outer loop controller of the rectifier is divided into two parts. One is in charge of regulating the output dc-link voltage. The other takes charge of maintaining the capacitor voltage balancing.

i. *DC-link voltage control*: To regulate the output dc-link voltage, a PI control is used here. The output of the PI controller is the reference for amplitude of input current. After getting the current amplitude, by combining the phase information from phase locking loop yields the input current reference. In a single-phase rectifier, its inherent ripple power at twice the grid frequency will result in second ripple on dc-link voltage. Also, the second voltage ripple may distort the input current of the rectifier further. To eliminate the negative effect, a notch filter with the notch frequency of 100 Hz is inserted as shown in Fig. 3.

ii. *Capacitor voltage balancing control:* Unbalanced capacitor voltages will degrade the system performance, so it is important to maintain the capacitor voltage balancing. The reasons for unbalanced capacitor voltages mainly are: (i) the used two capacitors are inconsistent; (ii) the sum of i_s and i_a contains dc components due to improper control. If the used capacitors are inconsistent, they will have different rate of self-discharge. Even if the sum of i_s and i_a do not contain any dc component, unbalanced capacitor voltage phenomenon will appear.

Assume that the system is steady state and i_s, i_a are expressed as

$$\begin{cases}i_s=I_p\sin\omega_it\\ i_a=I_m\sin\omega_ot\end{cases} \tag{20}$$

where I_p and ω_i denote the input current peak and angular frequency, and I_m and ω_o the stator current peak and angular frequency.

According to (2) and (3), the error of the two capacitor voltages is derived as

$$\Delta u=u_{dc12(0)}-\frac{I_p}{\omega_iC}\cos\omega_it-\frac{I_m}{\omega_oC}\cos\omega_ot \tag{21}$$

where $u_{dc12(0)}$ is the initial error of the two capacitor voltages.

From (21), the fluctuation in the error of the two capacitor voltages is inevitable. Thus, what we can do is to eliminate the dc component of the capacitor voltage error. Clearly, the second and the third term of (21) must be filtered out to abstract the dc component. The way to abstract the dc component is shown in Fig. 3, where two notch filters are used. Notch filter$_1$ is the same as that in dc-link voltage control; Notch filter$_2$ is a notch filter with the notch frequency being equal to ω_o. The abstracted dc component will be processed by the capacitor voltage balancing controller (PI), then a correction term Δi_s, which will revise the input current reference i_s^* to realise the capacitor voltage balancing is yielded. The revised input current reference current i_s^{**} is expressed as

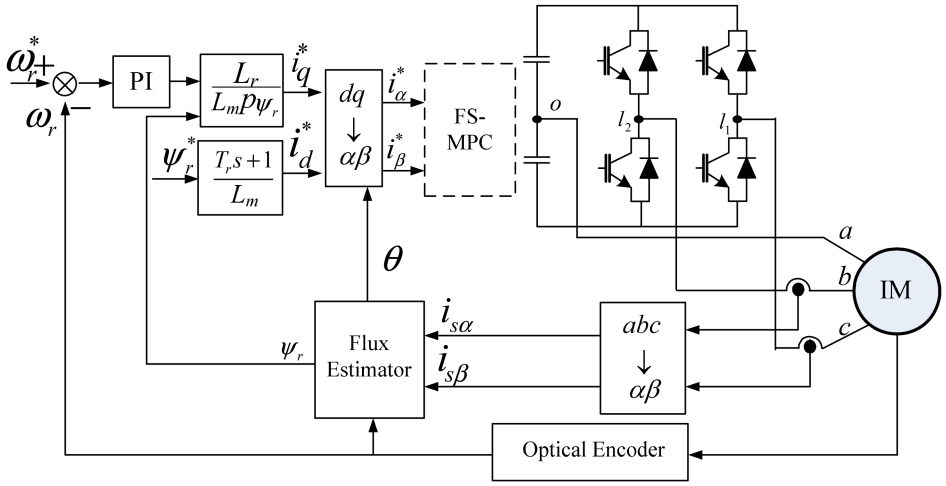

Fig. 4 *External loop control diagram of induction motor*

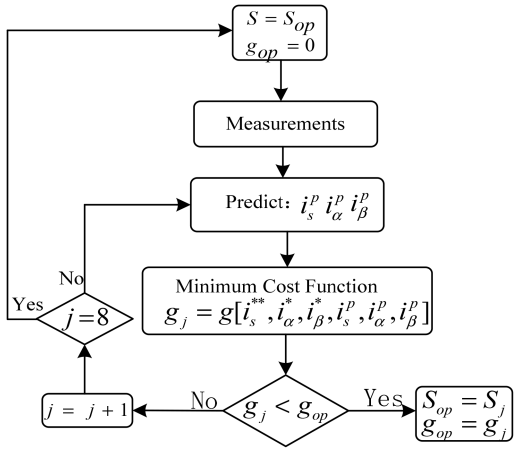

Fig. 5 *Flowchart of the predictive control*

$$i_s^{**} = i_s^* + \Delta i_s \tag{22}$$

iii. *Outer loop control for induction motor:* The outer loop control for induction motor is shown in Fig. 4, where the speed controller is a PI controller. The classic rotor field orientation control is used, thus the *dq*-coordinate system is aligned with the rotor flux to achieve the decoupling control of electromagnetic torque and rotor flux linkage.

4.2 Inner loop FS-MPC

FS-MPC is used to control the input current of the rectifier and the stator currents of the induction motor. There are two important steps in FS-MPC: establishing cost function and selecting optimal switching state. Based on the discretised model and the control objective, the cost function of the rectifier side can be set as

$$g_1 = |i_s^{**} - i_s^p|^2 \tag{23}$$

Similarly, the cost function of the inverter side is expressed as

$$g_2 = |i_\alpha^* - i_\alpha^p|^2 + |i_\beta^* - i_\beta^p|^2 \tag{24}$$

For this multi-objective optimisation problem, the weighted sum method is a simple and effective method. Therefore, g_1 and g_2 are added together to obtain the total minimum cost function

$$g = g_1 + \lambda g_2 \tag{25}$$

where λ is a weighting factor. The weighting factor is important for system performance. Usually, it is selected by trial and error method [25].

Since there are only eight possible switching combinations in this converter, and the computation burden is relatively low, the exhaust algorithm is used to obtain the optimal control. Fig. 5 shows the flowchart of the proposed algorithm.

Table 1 Parameters used in the simulations and experiments

Parameter	Value
input filtering inductance L	3 mH
input voltage	125 V(amplitude)
dc-link capacitor C_1,C_2	6800 μF
mutual inductance L_m	0.5 H
R_s, L_s	6.4 Ω, 0.5375 H
R_r, L_r	4.8 Ω, 0.5375 H
rated power	1.1 KW
rated voltage	380 V
rated current	2.89 A
rated angular speed	145.5 rad s^{-1}

5 Simulation and experimental research

5.1 Simulation results

In order to verify the feasibility and correctness of the hybrid predictive control for the system, some simulations have been carried out. The related parameters are listed in Table 1. The sampling period of the system is 40 μs, and the weighting factor in (25) is set to be $\lambda = 1.5$. The inertia, flux reference, and angular speed reference of IM are $J = 0.1$ kg m^2, $\psi_r^* = 0.96$ Wb, $\omega_r^* = 31$ rad s^{-1}, respectively.

The single-phase half-bridge rectifier converts the ac voltage of 125 V/50 Hz into the dc voltage of 300 V. The induction motor starts up without load and the load with torque $T_L = 4$ N m is connected at 0.6 s. In this case, the related simulation results are illustrated in Fig. 6. Fig. 6*a* shows the voltage and current waveforms of the single-phase grid in the steady-state operation. As seen, the unity power factor is almost realised in the rectifier. In Fig. 6*b*, the dc-link voltage is regulated at the desired value. Meanwhile, the capacitor voltage u_{dc1} and u_{dc2} are approximately the same, which means the midpoint voltage is balanced by the proposed control scheme. Fig. 6*c* illustrates the waveforms of stator currents. As seen, the starting current is three to four times higher than that in steady state. Since the motor is loaded at $t = 0.6$ s, the stator currents increase suddenly. Fig. 6*d* shows the waveforms of the angular speed and torque of the IM. It can be observed that the motor reaches the given angular speed before $t = 0.4$ s and then maintains a constant even with sudden load. The

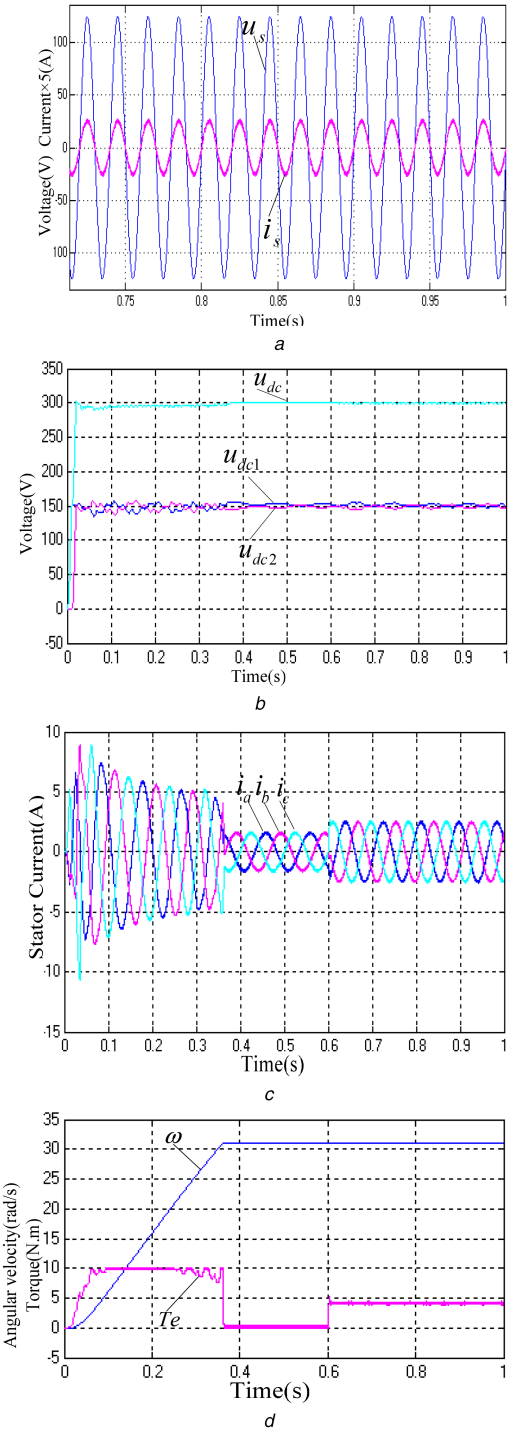

Fig. 6 *Simulation results of the system*

(a) Input voltage and input current, ***(b)*** Capacitor voltages, ***(c)*** Stator currents, ***(d)*** Speed and torque

torque curve shows that the starting torque is very large, then decreases gradually. When motor loads at $t = 0.6$ s, the electromagnetic torque rises to 4 N m, and the load torque is balanced.

To test the response of the dc-link voltage, a step change of dc-link voltage reference from 300 to 400 V is made at $t = 0.4$ s. The simulation results are shown in Fig. 7. As shown in Fig. 7*a*, the capacitor voltages reach a new steady-state quickly. Also, the two capacitors voltage waveforms are nearly coincided with each other, which demonstrates the feasibility of the proposed voltage balancing control scheme.

From Figs. 7*b* and *c*, it can be seen that the sinusoidal steady stator currents and torque of low ripple are obtained under the proposed control scheme.

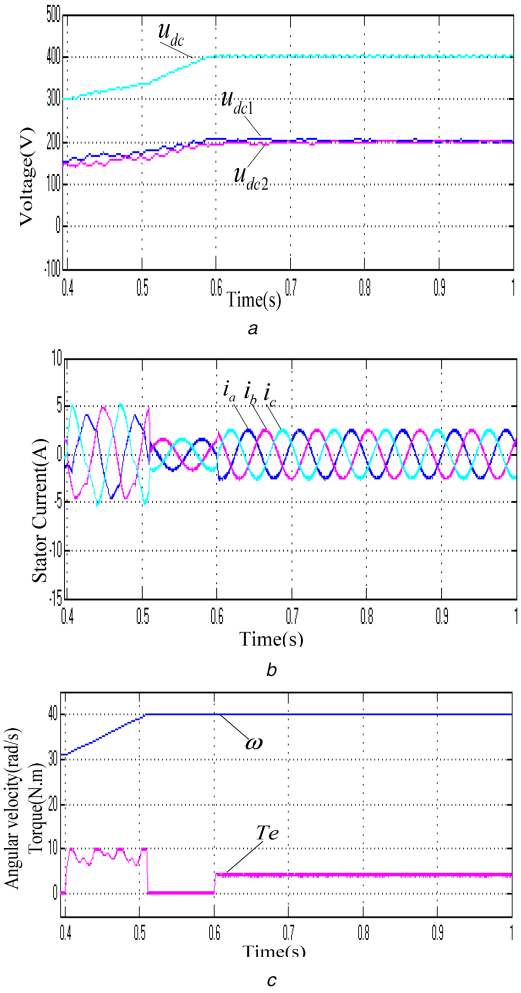

Fig. 7 *Simulation result with step change of dc-link voltage from 300 to 400 V*

(a) Capacitor voltages, ***(b)*** Stator currents, ***(c)*** Speed and torque

5.2 Experimental results

The proposed control algorithm is implemented in a TMS320F28335 DSP controller board. The parameters of the experimental system are the same with those in simulation and are shown in Table 1. The single-phase half-bridge rectifier is connected to the power grid through an auto-transformer, and the three-phase induction motor is driven by the three-phase four-switch inverter. Also, the dc-link voltage reference is set to 300 V. The motor starts up at no-load, after 0.35 s, a load of 4 N m is connected to it. The measured experimental waveforms are shown in Fig. 8. Fig. 8*a* shows the waveforms of the voltage and current of the grid. It can be seen that the grid current is in phase with the grid voltage; the unit power factor is basically realised.

The measured voltages of the two capacitors are shown in Fig. 8*b*. At first, the voltage on the capacitors C_1 and C_2 is maintained at 125 V by the uncontrolled diode rectifier. During start up, the voltage increase from 125 to 150 V gradually, which makes the total dc-link voltage follow its expected value of 300 V.

Figs. 8*c* and *d* show the experimental results of the induction motor, which agree well with those in the simulations. The speed is well controlled without any overshoot. The three-phase stator currents are sinusoidal, and the response of stator currents to sudden loads is very fast due to the predictive control. Meanwhile, the torque ripple is small in steady state.

The grid current and stator currents are analysed and the results are given in Table 2. The THDs are relatively low within 5% indicating the good performance of the proposed scheme.

To test the dynamic response of the dc-link voltage, its reference is changed from 300 to 400 V at $t = 0.8$ s. At the same time, the speed reference is changed from 38 to 52 rad s^{-1} at $t = 0.8$ s. The motor is loaded with the torque of 4 N m at $t = 2$ s. The

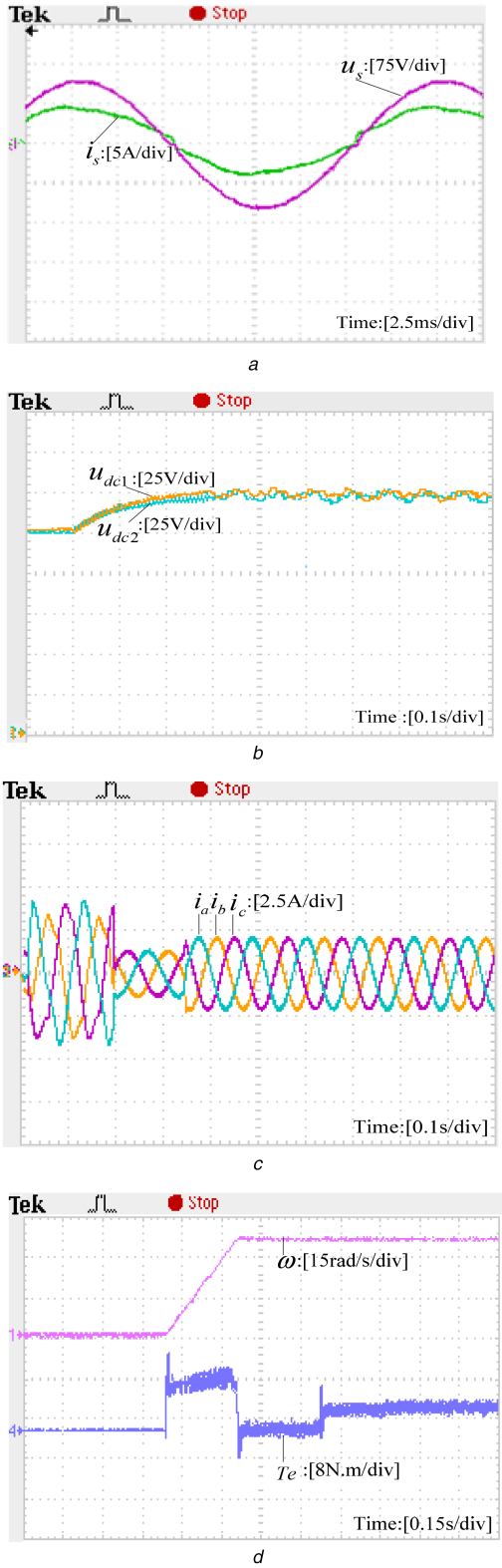

Fig. 8 *Experimental results of hybrid predictive control for the low-cost converter*

(a) Input voltage and current, ***(b)*** Capacitor voltages, ***(c)*** Three-phase stator currents, ***(d)*** Speed and torque

Table 2 THD and RMS value of the grid and stator currents

Grid current i_s and stator currents i_a, i_b, i_c	i_s	i_a	i_b	i_c
THD, %	3.93	3.06	3.65	3.29
RMS, A	3.23	1.45	1.40	1.42

corresponding experimental results are illustrated in Figs. 9*a* and *b*. As seen, the angular speed reaches 38 rad s^{-1} firstly and then runs

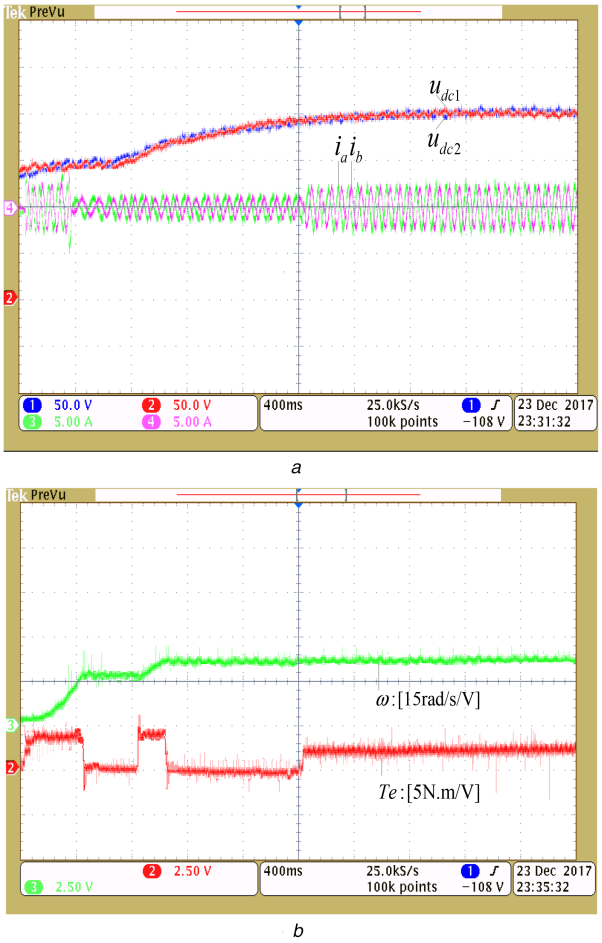

Fig. 9 *Experimental results when the dc-link voltage reference is changed from 300 to 400 V*

(a) Capacitor voltages and stator currents, ***(b)*** Speed and torque

at 52 rad s^{-1} steadily. Besides, the overshoot of angular speed is very small. The torque curve shows that the starting torque of the motor is very large, then decreases gradually. When motor loads at $t = 2$ s, the electromagnetic torque rises to 4 N m to balance the load torque. The proposed control strategy shows good stator phase current waveforms. Here, it can be appreciated that the two capacitor voltages change to a new steady-state values. Moreover, the two capacitor voltage waveforms are nearly coincided with each other, which has demonstrated the dc-link two capacitor voltages is balanced when the dc-link voltage reference changes.

6 Conclusions

In this paper, a hybrid predictive control strategy is proposed, which is a combination of PI control and FS-MPC. The simulation and experimental results show that the proposed control scheme can achieve the multi-objective control efficiently. Compared with the traditional control schemes, the major advantages of the method include: (i) easy to deal with complicated constraints and manage multiple control targets; (ii) without the need of PWM modulator; (iii) good dynamic response; (iv) the computation burden is relatively low. The proposed control idea can also be applied to other drive systems.

7 Acknowledgments

This work was supported by the National Nature Science Foundation of China under Grant no. 61573382, and the Natural Science Foundation of Hunan Province of China under Grant no. 2016TP1023.

7 References

[1] Welchko, B.A., Lipo, T.A., Jahns, T.M., *et al.*: 'Fault tolerant three-phase AC motor drive topologies: a comparison of features, cost, and limitation', *IEEE Trans. Power Electron.*, 2004, **19**, (4), pp. 1108–1116

[2] Jacobina, C.B., Correa, M.B., de, R.:'AC/AC converters with a reduced number of switches'. Proc. Int. Conf. Industry Application, Chicago, USA, September 2001, pp. 1755–1762

[3] Zhou, D.H., Zhao, J., Liu, Y.: 'Finite control set model predictive control scheme of three-phase four-leg back-to-back converter-fed induction motor drive', *IET Electr. Power Appl.*, 2017, **11**, (5), pp. 761–767

[4] Jacobina, C.B., de Freitas, I.S., Lima, A.M.N., *et al.*: 'DC-link three-phase-to-three-phase four-leg converters', *IEEE Trans. Ind. Electron.*, 2007, **54**, (4), pp. 1953–1961

[5] Soeiro, T.B., Kolar, J.W.: 'Analysis of high-efficiency three-phase two-and three-level unidirectional hybrid rectifiers', *IEEE Trans. Ind. Electron.*, 2013, **60**, (9), pp. 3589–3601

[6] Wei, Z., Chen, J., Chen, X., *et al.*: 'Modified one-cycle-controlled three-phase pulse-width modulation rectifiers under low-output DC voltage conditions', *IET Power Electron.*, 2014, **7**, (9), pp. 753–763

[7] Wang, B., Venkataramanan, G., Bendre, A.: 'Unity power factor control for three-phase three-level rectifiers without current sensors', *IEEE Trans. Ind. Appl.*, 2007, **43**, (5), pp. 1341–1348

[8] de Rossiter Correa, M.B., Jacobina, C.B., da Silva, E.R.C., *et al.*: 'A general PWM strategy for four-switch three-phase inverters', *IEEE Trans. Power Electron.*, 2006, **21**, (6), pp. 1618–1627

[9] Kazmierkowski, M.P., Malesani, L.: 'Current control techniques for three-phase voltage-source PWM converters: a survey', *IEEE Trans. Ind. Electron.*, 1998, **45**, (5), pp. 691–703

[10] Dzung, P.Q., Phuong, L.M., Vinh, P.Q.: 'New space vector Control approach for four switch three phase inverter (FSTPI)'. Proc. Int. Conf. Power Electronics and Drive Systems, Bangkok, Thailand, November 2007, pp. 1002–1008

[11] Blaabjerg, F., Freysson, S., Hansen, H.H., *et al.*: 'Comparison of a space-vector modulation strategy for a three phase standard and a component minimized voltage source inverter'. Proc. Int. Conf. EPE, Seville, Spain, September 1995, pp. 1806–1813

[12] Hwang, S.H., Kim, J.M.: 'Dead time compensation method for voltage-fed PWM inverter', *IEEE Trans. Energy Convers.*, 2010, **25**, (1), pp. 1–10

[13] Ahmadi, D., Wang, J.: 'Selective harmonic elimination for multilevel inverters with unbalanced DC inputs'. Proc. Int. Conf. Vehicle Power and Propulsion, Dearborn, USA, September 2009, pp. 773–778

[14] Blaabjerg, F., Neacsu, D.O., Pedersen, J.K.: 'Adaptive SVM to compensate DC-link voltage ripple for four-switch three-phase voltage-source inverters', *IEEE Trans. Power Electron.*, 1999, **14**, (1), pp. 743–752

[15] Kim, J., Nam, K.: 'A current distortion compensation scheme for four-switch inverters', *IEEE Trans. Power Electron.*, 2009, **24**, (6), pp. 1032–1040

[16] Lee, D.M., Park, J.B., Toliyat, H.A.: 'A simple current ripple reduction method for B4 inverters', *J. Elect. Eng. Technol.*, 2013, **8**, pp. 1062–1069

[17] Morari, M., Lee, J.H.: 'Model predictive control: past, present and future', *Comput. Chem. Eng..*, 1999, **23**, (4), pp. 667–682

[18] Dan, H., Zhu, Q., Peng, T., *et al.*: 'Preselection algorithm based on predictive control for direct matrix converter', *IET Electr. Power Appl.*, 2017, **11**, (5), pp. 768–775

[19] Cheng, K., Jen, T., Li, C.: 'Model-free predictive current controller for four-switch three-phase inverter-fed interior permanent magnet synchronous motor drive systems'. Proc. Int. Conf. Advanced Intelligent Mechatronics, Kachsiung, Taiwan, July 2012, pp. 1048–1053

[20] Vargas, R., Rodríguez, J., *et al.*: 'Predictive current control of an induction machine fed by a matrix converter with reactive power control', *IEEE Trans. Ind. Electron.*, 2008, **55**, (12), pp. 4362–4371

[21] Formentini, A., Trentin, A., Marchesoni, M., *et al.*: 'Speed finite control set model predictive control of a PMSM fed by matrix converter', *IEEE Trans. Ind. Electron.*, 2015, **62**, (11), pp. 6786–6796

[22] Montanari, M., Peresada, S., Tilli, A.: 'A speed-sensorless indirect field-oriented control for induction motors based on high gain speed estimation', *Automatica*, 2006, **42**, (10), pp. 1637–1650

[23] Habibullah, M., Lu, D.C.: 'Predictive torque and flux control of a four-switch inverter-fed IM drive'. Proc. Int. Conf. Int. Future Energy Electronics, Tainan, Taiwan, November 2013, pp. 629–634

[24] Zhu, C., Zeng, Z.Y., Zhao, R.X.: 'Comprehensive analysis and reduction of torque ripples in three-phase four-switch inverter-fed PMSM drives using space vector pulse-width modulation', *IEEE Trans. Power Electron.*, 2017, **32**, (7), pp. 5411–5424

[25] Cortes, P., Kouro, S., Rocca, B.L., *et al.*: 'Guidelines for weighting factors design in model predictive control of power converters and drives'. Proc. Int. Conf. IEEE ICIT, Gippsland, VIC, Australia, February 2009, pp. 1–7